[Short title + Author Name - P&H title] 17 (2024) 105735

Contents lists available at ScienceDirect

Arabian Journal of Chemistry

journal homepage: www.ksu.edu.sa

Cationic anticancer peptide L-K6-modified and doxorubicin-loaded mesoporous silica nanoparticles reverse multidrug resistance of breast cancer

Haiting Sun [a,b,1], Shaodan Dong [a,d,1], Lingying Kong [a], Rongchun Wang [a], Jiaqi Zhao [a], Yue Guan [b,c], Che Wang [a,b,*], Dejing Shang [b,c,*]

[a] Department of Medicinal Chemistry, School of Chemistry and Chemical Engineering, Liaoning Normal University, Dalian 116029, China
[b] Liaoning Provincial Key Laboratory of Biotechnology and Drug Discovery, Liaoning Normal University, Dalian 116081, China
[c] School of Life Science, Liaoning Normal University, Dalian 116081, China
[d] Zhuanghe No.30 Junior Middle School, Dalian 116499, China

ARTICLE INFO

Keywords:
Cationic anticancer peptide
Doxorubicin
MCF-7/ADR
Mesoporous silica nanoparticle
Multidrug resistance

ABSTRACT

Multidrug resistance (MDR) is the major challenge for chemotherapy of cancer and makes the treatment benefits unsustainable. To overcome this issue, nanotechnology has been introduced and various nanocarriers have been constructed to reverse MDR in drug resistant cancer cells. Here, mesoporous silica nanoparticle (MSN-COOH) were modified with cationic anticancer peptide L-K6 (MSN@L-K6), and further loaded with doxorubicin (DOX) to construct an anticancer nano-system, MSN@L-K6@DOX. Our results showed that MSN@L-K6@DOX released DOX in pH-sensitive manner, which enable to be highly efficient in delivering drugs to tumors, counterbalancing the MDR. In addition, MSN@L-K6@DOX treatment decreased the expression level of P-glycoprotein in MCF-7/ADR cells, enhanced the intracellular accumulation of DOX, and thereafter reversed the MDR of MCF-7/ADR cells to DOX. Moreover, the MDR reversal activity of MSN@L-K6@DOX was further confirmed in xenograft mouse model, as evidenced by the decreased tumor volume and weight. These results indicate the MDR reversal activity of MSN@L-K6@DOX and may provide a novel strategy for the development of nano-based drug delivery system to overcome cancer MDR.

1. Introduction

Cancer is a major public health challenge worldwide and is the second leading cause of death in the United States (Siegel et al., 2021). Despite the significant advances in the diagnosis and chemical or biological therapies of cancer, the development of multidrug resistance (MDR) is still a major obstacle to effective cancer therapy (Jemal et al., 2009; Szakács et al., 2006). MDR refers to the phenomenon of cross-resistance to a variety of drugs with different structures, targets and mechanisms of action. There are two sources of MDR, one is endogenous, itself exists in the tumor cells; the other is exogenously acquired and is usually associated with overexpression of P-glycoprotein (P-gp) or other efflux pump proteins, leading to reduced drug uptake, altered DNA repair, and drug resistance. Both types seriously affect the action of anticancer drugs (Duan et al., 2023), therefore, discovery and development of novel biomaterials or therapeutic candidates with MDR reversal activity will help improve the clinical benefits of conventional anticancer therapy.

The development of MDR in tumor cells is mainly caused by the overexpression of P-gP on the cell membrane, and in order to reverse MDR in cancer cells, some organic nano-based drug delivery systems such as liposomes, lipid nanoparticles, polymer-based nanoparticles and micelles have been constructed to bypass the specific efflux proteins and increase intracellular drugs accumulation in cancer cells (Li et al., 2019; Cao et al., 2019; Zhao et al., 2015; Wang et al., 2014). However, these organic nano carriers easily suffer from various biochemical attacks and bioerosions owing to their inherent instability in vivo (Shen et al., 2011).

Recently, increasing lines of evidence has indicated that inorganic mesoporous silica nanoparticles (MSNs) has a promising potential as

* Corresponding authors.
E-mail addresses: wangche126@lnnu.edu.cn (C. Wang), djshang@lnnu.edu.cn (D. Shang).
[1] These two authors contributed equally to this work.

https://doi.org/10.1016/j.arabjc.2024.105735
Received 20 September 2023; Accepted 15 March 2024
Available online 16 March 2024

safe and effective drug delivery system due to their excellent in vivo stability. MSNs have been intensively investigated in various fields including drug delivery, biosignal probing, gene delivery, and biomarking (Huo, 2011). Compared with organic drug carriers, MSNs possess some unique properties such as high specific surface area, large pore volume, tunable pore structure and stable physicochemical properties, therefore have been investigated as drug delivery vectors to deliver siRNA and other chemotherapeutic agents into cancer cells to overcome MDR (Shen et al., 2011; Xu et al., 2006; Varshosaz and Taymouri, 2015). However, the intracellular drugs delivered by MSNs can still be actively exported out of cancer cells by efflux proteins, such as P-glycoprotein (P-gP), before their entering into cell nucleus to kill cancer cells. Therefore, functional modifications on MSNs to inhibit P-gP and to strengthen their MDR reversal activity are urgently needed.

Functionally modified MSNs drug-carrying systems are mainly environmentally responsive nanomaterials, with the most common environmental factors include light, magnetism, enzymes, competitive reactions, temperature and pH, etc., of which pH-sensitive occupies a major role in biomedical field (Hu et al., 2017). In MSNs drugs carrying system, chemotherapeutic drugs are commonly loaded onto the nanocarriers through electrostatic attraction, which was weakened under acidic condition, leading to the increased release of chemotherapeutic drugs. Actually, the extracellular pH of tumor tissues (pH = 6.8) is maintained below normal non-cancerous tissues, and the pH of intracellular endosomes and lysosomes of tumor cells are even much lower (pH < 5.4) (Zeng et al., 2017), therefore pH-sensitive carriers can serve as a highly efficient tool for delivering drugs to tumors compared to conventional nanoparticles. In addition, while these pH-sensitive mesoporous silica-carrying systems can be taken up by cells through endocytosis, more chemotherapeutic drugs can be released under the intracellular acidic conditions to counterbalance the P-gP mediated cancer MDR (Huang et al., 2011).

Previous studies have found that the diameter of functionally-modified nanocarriers is less than 200 nm, which can effectively target tumor tissues in vivo by enhancing permeability and retention effect. The smaller the diameter, the better the tumor targeting and permeability (Murugan et al., 2016). At the same time, carboxyl modified MSNs (MSNs-COOH) have high specific surface area and pore volume, which can not only enhance the surface hydrophilicity of MSNs, but also make the materials pH sensitive. Much more importantly, modifications of MSNs using functional groups with P-gP inhibiting activity have also been reported to strengthen the delivery efficiency and anticancer activity of nanocarriers (Pan et al., 2021; Halder et al., 2022).

We previously found that one cationic anticancer peptide L-K6 can inhibit P-gP expression in MCF-7/ADR cell (Wang et al., 2021). In an endeavor to develop advanced drug delivery system with enhanced chemotherapy to overcome MDR in breast cancers, in the present study, we constructed a functional MSN delivery system modified with L-K6 and loaded with doxorubicin (DOX) by electrostatic action for synergistic therapy of MDR cancer cells (Suppl. Fig. S1). The cationic property and P-gP inhibiting activity may favor the delivery system to interact preferentially with cancer cells and delivery DOX efficiently into MDR cells. Carboxyl MSNs (MSN-COOH) were conjugated with L-K6 (MSN@L-K6) and subsequently loaded with chemotherapy drug DOX by encapsulation into the channel of MSNs to construct MSN nanocarrier, namely as MSN@L-K6@DOX. The in vitro cytotoxicity and MDR reversal activity of MSN@L-K6@DOX were evaluated in MCF-7/ADR cells and was further confirmed in vivo by xenograft model mice.

2. Materials and methods

2.1. Chemicals, cell lines and animals

3-ethylcarbodiimide hydrochloride (EDC·HCl), N-hydroxysuccinimide (NHS), and 3-[4,5-dimethylthiazol-2-yl]-2,5 diphenyl tetrazolium bromide (MTT) were purchased from Sigma-Aldrich (St. Louis, MO, USA). DOX was provided by Dalian Meilun Biotech Co., Ltd. (Dalian, China). All other chemicals used in the present study were commercially available and used as received.

MCF-7 and MCF-7/ADR cell lines were obtained from the CBCAS (Cell Bank of the Chinese Academy of Sciences, Shanghai, China). Cells were routinely cultured in DMEM/F12 medium containing 10 % fetal bovine serum (FBS), 1 % l-glutamine, 1 % sodium pyruvate, 50 U/mL penicillin and 50 μg/mL streptomycin. The cells were maintained at 37 °C in a humidified atmosphere of 5 % CO_2.

Female Balb/c nude mice with average weight of 20 g (6–8 weeks of age) were purchased from Vital River Laboratories (Beijing, China). MCF-7/ADR cell xenograft tumor model was established according to our previous protocol (Dong et al., 2020). MCF-7/ADR cells were collected by centrifugation and dispersion in 100 μL sterilized saline at 2 × 10^7 cells/mL density and subcutaneously injected into the right flank next to the forelimb of nude mice. As for the anticancer effects assessment, when the tumor volume reached 50 mm^3, the animals were randomized into four groups (six mice per group): (1) saline control group, (2) free DOX group, (3) MSN@DOX group, and (4) MSN@L-K6@DOX. Animals were injected intravenously (i.v.) via the tail vein with 200 μL of sterile saline, free DOX, MSN@DOX, and MSN@L-K6@DOX (at a dose normalized to be 100 mg/kg DOX equiv), respectively. Each treatment was performed four times at 3-day intervals (days 1, 4, 7, 10). The body weight and tumor size of each mouse were recorded every 2 days. All experiments procedures were performed in accordance with the Laboratory Animal Care and Use Guidelines approved by the Animal Care and Use Committee of Liaoning Normal University.

2.2. Preparations of MSN-COOH and MSN@L-K6

MSN-COOH was synthesized according to the previously reported method (Ding et al., 2015). MSN (5 mg) and succinic anhydride (3 mg) were dispersed in N,N-dimethylformamide and stirred overnight. The products were then purified by centrifugation to remove excess succinic anhydride. The deposition was ultrasonically dispersed in PBS (pH = 5.3), stirred with EDC (23.0 mg, 0.12 mmol) and NHS (13.8 mg, 0.12 mmol) at room temperature for 24 h, then washed and dispersed in PBS (pH = 7.4). The pellet was re-suspended in methanol and washed at 10,000 rpm for 40 min, followed by washing with distilled water. These washing steps were repeated twice with sonication at each step for re-suspension. The yielded MSN-COOH was dried by desiccation. As for the preparation of MSN@L-K6 nanocarrier, L-K6 peptide (1 mL, 1 mg/mL) was added into MSN-COOH and stirred for 24 h.

2.3. DOX loading

For DOX loading, 1 mg of MSN-COOH or MSN@L-K6 was mixed with 1 mL of DOX solution in PBS (pH = 7.4, 6.8, and 5.4, 1 mg/mL) and stirred for 24 h at room temperature in the dark. The loading mixture was centrifuged at 9000 rpm for 15 min to collect the DOX loaded nanocarriers. Amount of DOX in the supernatant was estimated by UV–vis Spectrophotometer (Nanodrop-2000C, ThermoFisher, USA). By comparing the absorbance of DOX in the supernatants with the calibration curves of DOX (obtained at the same conditions, diverse concentrations in the range of about 5–50 ppm), the load content and drug entrapment efficiency were calculated.

2.4. Characterization of MSNs nanocarrier

The size, size distribution, and zeta potential of various nanomaterials were analyzed using a Delsa Nano photon correlation spectroscopy (PCS, Beckman Coulter, USA). The surface morphology was observed by transmission electron microscopy (TEM, Tecnai G2 20, FEI Company, Hillsboro, Oregon, USA). A Fourier transform infrared spectroscopy (FT-IR, TENSOR27, Bruker, Germany) was used to analyze

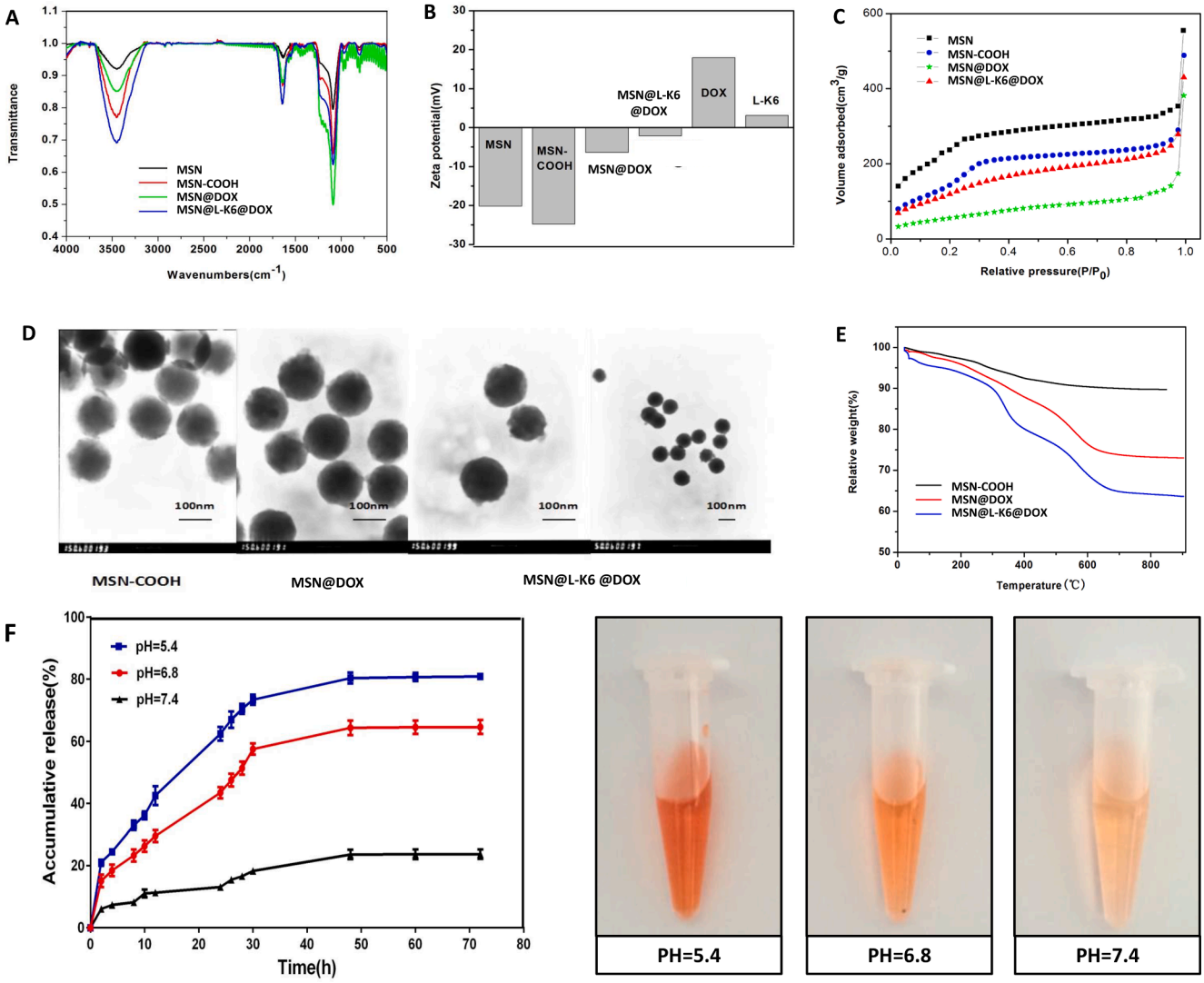

Fig. 1. Characterizations of functionalized MSNs. (A) Fourier-transform infrared spectroscopy assay; (B) Surface charge potentials of different functionalized MSNs as assessed by the zeta potential analysis; (C) Nitrogen adsorption–desorption isotherm analysis; (D) The transmission electron microscopy images of MSNs nanoparticles before and after drug loading; (E) The thermogravimetric analysis. **(F)** Accumulative release of DOX from MSN@L-K6@DOX under different pH conditions.

Table 1
The parameters of mesoporous silica nanoparticles (MSNs).

Sample	BET surface Area (m^2/g)	Pore Volume (cm^3/g)	Pore Size (nm)	NPs size (nm)	Zeta Potential (mV)
MSN	1052.6 ± 75.1	0.96 ± 0.04	2.974 ± 0.162	107.23 ± 1.79	0
MSN-COOH	632.2 ± 42.4	0.93 ± 0.03	2.970 ± 0.151	113.41 ± 3.17	−24.07 ± 0.69
MSN@L-K6	210.8 ± 15.6	0.76 ± 0.02	2.741 ± 0.169	127.43 ± 4.36	−18.51 ± 0.15
MSN@L-K6@DOX	480.8 ± 28.2	0.32 ± 0.03	1.154 ± 0.137	150.78 ± 1.07	2.72 ± 0.54

Table 2
The MSN@DOX@L-K6 of drug loading and entrapment efficiency.

pH	Drug loading (%)	Encapsulation efficiency (%)
7.4	28.47 %	69.36 %
6.8	22.65 %	56.37 %
5.4	13.41 %	31.32 %

functional groups present in the MSNs. FT-IR spectra were obtained in the range of 400–4000 cm^{-1}. Thermal gravity analyzer (TGA, PerkinElmer, USA) was used to characterize MSNs by heating the sample to 800 °C (20 °C min^{-1}). N_2 adsorption/desorption isotherm analysis was performed at −196 °C by an absorption analyzer (ASAP 2020, Micromeritics, USA), and the degassing temperature is 120 °C. The specific surface area and pore size were calculated by BET and BJH method, respectively.

2.5. *In vitro drug release*

The above-prepared MSN@L-K6@DOX (1 mg) in a 10,000 Ka dialysis bag was immersed in 20 mL PBS (pH 7.4, 6.8 or 5.4), with stirring at room temperature. At certain time intervals, 8 mL of the release medium were taken out for testing DOX concentrations by UV/vis spectroscopy at wavelength of 483 nm. The absorbance of supernatant was recorded.

2.6. *Cellular uptake assessment of DOX-loaded MSNs*

The MCF-7/ADR cells were seeded in 12-well plate with cover slips at 5×10^5 cells density. After 24 h incubation, different concentrations (10, 20, 40 and 80 μg/mL) of free DOX, MSN@DOX or MSN@L-

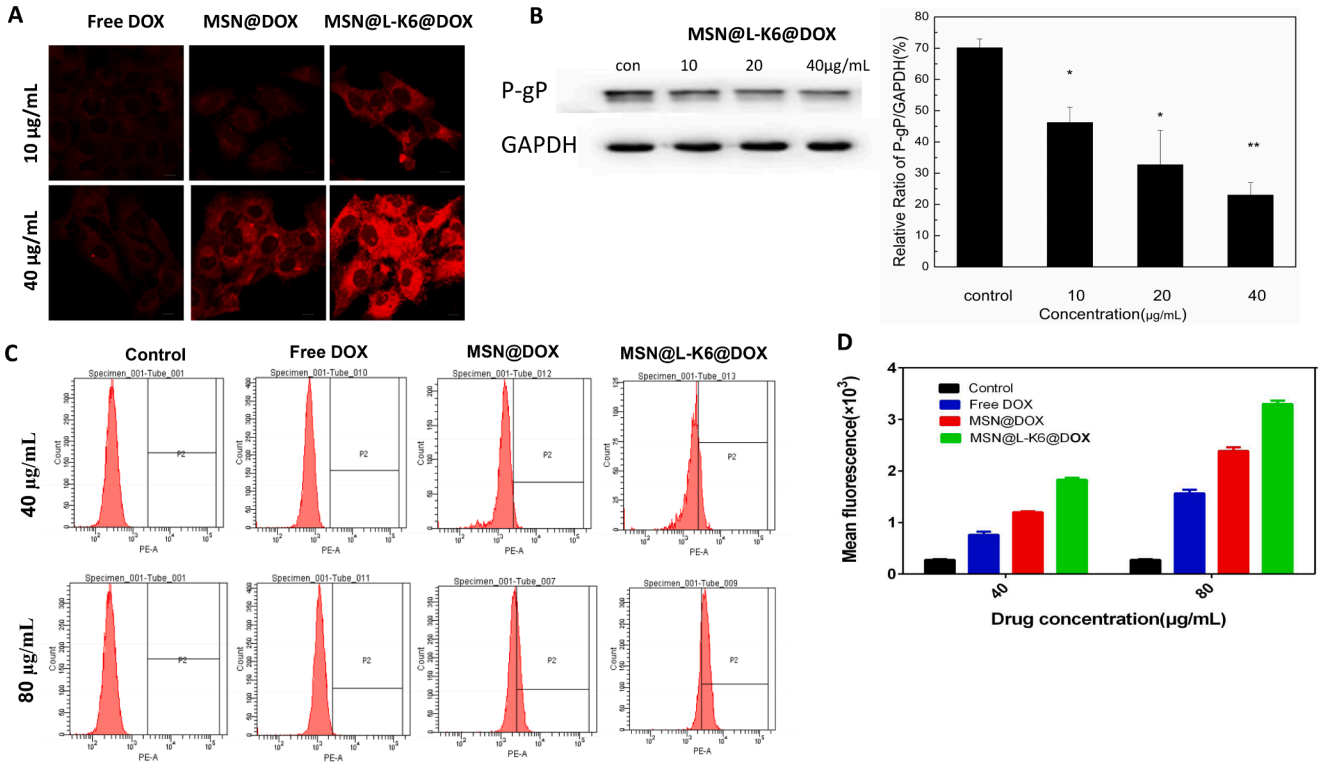

Fig. 2. Intracellular DOX accumulation and P-gP inhibition after functionalized MSNs exposure in MCF-7/ADR cells. (A) Confocal laser scanning microscopy images of MCF-7/ADR cells incubated with MSN@DOX and MSN@L-K6@DOX at different concentrations (10 μg/mL and 40 μg/mL) after 24 h; (B) P-gP expression level in MCF-7/ADR cells after 24 h MSNs exposure. (C) Flow cytometric analysis and (D) quantitative analysis of the cellular DOX uptake in MSNs treated MCF-7/ADR cells.

K6@DOX were added and co-incubated for 24 h at 37 °C. After incubation, culture medium was removed and cells were washed with PBS thrice. Then, cells were fixed by 4 % paraformaldehyde (PFA), washed with PBS and mounted on slides with 80 % glycerol. The intracellular fluorescence of DOX was imaged using confocal microscope (Zeizz LSM 710, Zeizz Instruments Co., Germany).

Cellular uptake by MCF-7/ADR cells was confirmed using flow cytometry. The cells were seeded in 6-well culture plates (8×10^5 cells/well) and allowed to grow for 24 h. Free DOX, MSN@DOX or MSN@L-K6@DOX were added into cells for 24 h incubation. Then, cells were washed, centrifuged, and fixed in 4 % PFA (in PBS). Cells were re-suspended in PBS and the intracellular fluorescence was analyzed using flow cytometer (FACS callibur, BD Bioscience, USA).

2.7. In vitro cytotoxicity assessment by MTT assay

In vitro cytotoxicity was evaluated by MTT assay. MCF-7/ADR cells were seeded in 96-well plate at a density of 5×10^4 cells/well and cultured for 24 h. Then free DOX, MSN-COOH, MSN@DOX, and MSN@L-K6@DOX were dispersed in complete medium and added into the wells with final concentrations of 10, 20, 40, 80 and 160 μg of DOX/mL. After incubation, 10 μL of MTT (5 mg/mL) was added to each well and incubated for 4 h at 37 °C. Following incubation, medium with MTT was removed, and 150 μL of DMSO was added to solubilize formazan crystals.

2.8. Tumor xenograft models and treatments

All animals care and experiments were performed in compliance with the Guidelines for the Care and Use of Laboratory Animals and all procedures were approved by the Animal Care and Use Committee of Liaoning Normal University. To set up the tumor xenograft model, the female BALB/C nude mice (6 weeks, 18 ~ 22 g, purchased from Nanjing Biomedical Research Institute of Nanjing University) were subcutaneously inoculated in the right axilla with 10^7 MCF-7/ADR cells (200 μL/mouse). The tumor size was monitored by a vernier calliper and the tumor volume (V) was calculated as $V = L \times W2/2$, where L and W were the length and width of the tumor, respectively. When the tumors reached to 100 ~ 150 mm^3, the mice were randomized into 4 groups: control group, DOX group, MSN@DOX group and MSN@L-K6@DOX group, intravenously injected by sterile saline, DOX (5 mg/kg), MSN@DOX (5 mg/kg), and MSN@L-K6@DOX (5 mg/kg), respectively. The injection was performed every two days on day 1, 3, 5, 7 and 9. The body weight and tumor volume were recorded. The DOX distribution was monitored by in vivo imaging, based on the endogenous fluorescence property of DOX. As for the in vivo imaging observation, images were taken once daily for 14 consecutive days on IVIS® Lumina III imaging system (PerkinElmer, USA, excitation: 748 nm, emmision: 780 nm) 2 h post injection. After final scanning, the mice were euthanized and sacrificed. The tumor tissues were harvested and weighted.

2.9. Statistical analysis

The results are expressed as the means and standard errors. A paired Student's *t*-test was used to determine the significance of difference between groups. Significance is indicated as fellows: $^*p < 0.05$, $^{**}p < 0.01$, $^{***}p < 0.001$.

3. Results and discussion

3.1. Characterization of MSN-COOH, MSN@DOX and MSN @DOX@L-K6

FT-IR was used to identify the chemical functional groups of MSN-COOH and MSN@L-K6 surface (Fig. 1**A**). Weak absorption peaks of Si-OH bending vibration can be observed at 970 cm^{-1}, whereas a strong absorption peak of Si-O-Si antisymmetric stretching vibration was found at 1,092 cm^{-1}. Worth noting, at 1,648 cm^{-1} wavelength, a typical

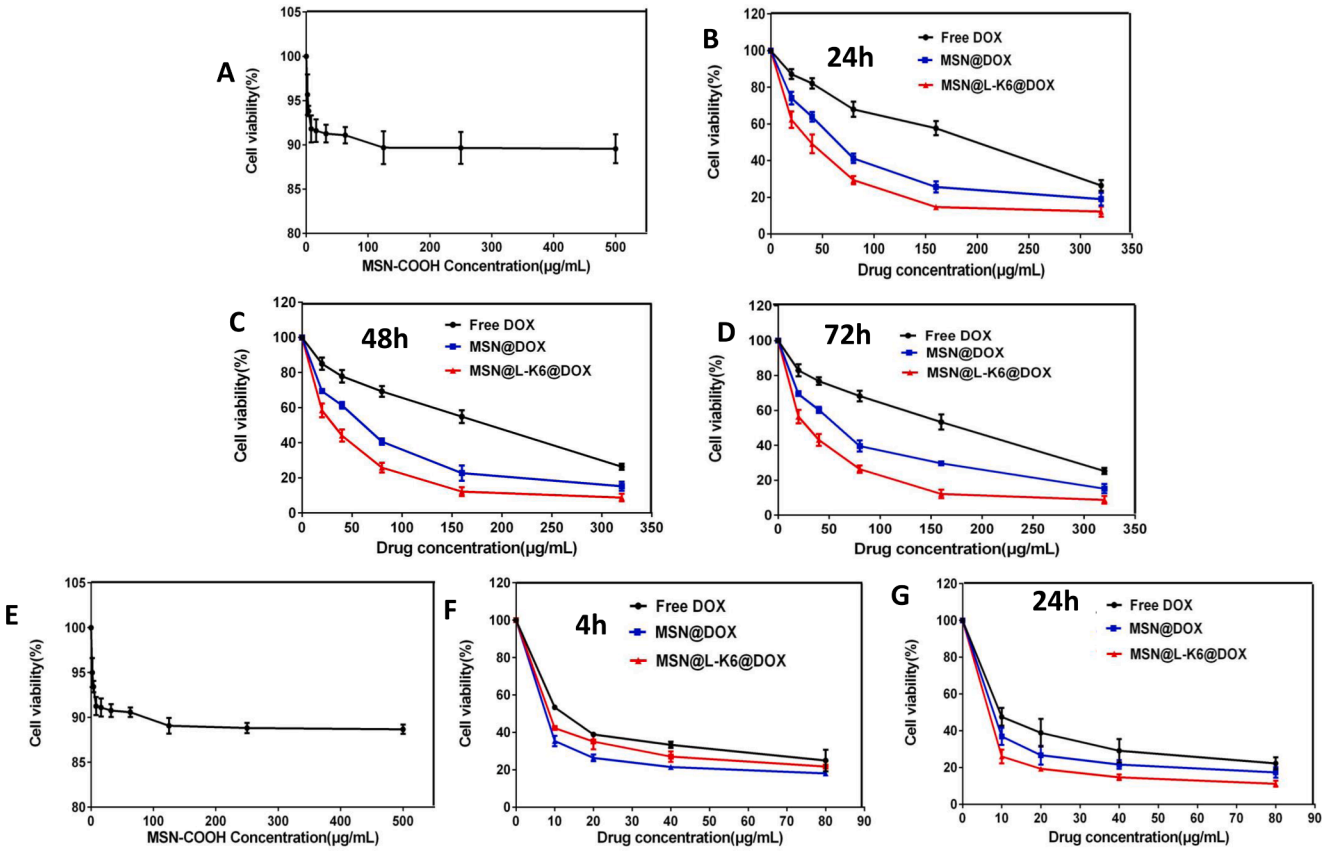

Fig. 3. MCF-7/ADR and MCF-7 cell viability after DOX and MSNs exposure (A) Cell viability after exposure of various concentrations (5 to 500 μg/mL) of MSN-COOH for 24 h. (B-D) In vitro viability of MCF-7/ADR cells after 24, 48, and 72 h incubation with MSN@DOX, MSN@L-K6@DOX, or free DOX. (E) MCF-7 cell viability after exposure of various concentrations (5 to 500 μg/mL) of MSN-COOH for 24 h. (F, G) In vitro viability of MCF-7 cells after 4 h and 24 h, incubation with MSN@DOX, MSN@L-K6@DOX, or free DOX.

carboxyl absorption peak in MSN-COOH was presented, which confirmed the success of carboxyl functionalization. In addition, the peak at 1,642 cm^{-1} corresponding to the characteristic bending of $–NH_2$ and another asymmetric peak at 3,486 cm^{-1} attributed to -N-H stretching in MSN@L-K6, which indicated the conjugation of L-K6 with MSN-COOH surface.

Additionally, as shown in Fig. 1**B**, the zeta potential analysis indicated that MSN-COOH showed a negative potential at –23.89 mV. In contrast, DOX showed a positive potential of 20.13 mV. Hence, after DOX loading, zeta potential value of MSN@DOX was increased to −6.77 mV, but still under the negative level. L-K6 also showed a positive charge of 5.89 mV. Therefore, the L-K6 and DOX dually loaded MSN@L-K6@DOX system showed a further reduced negative charge as 2.58 mV (Fig. 1**B**).

N_2 adsorption–desorption isotherms analysis (Fig. 1**C**) and TEM observation (Fig. 1**D**) indicated that MSNs and MSN-COOH presented a moderate size of 100 nm. The results demonstrated that MSN-COOH exhibited uniform mesoporous nanostructure but with a slight decrease on specific surface area (632 m^2/g) and average pore size (2.970 nm) as compare to MSN (1052.673 m^2/g and 2.974 nm, respectively, Table 1). Nevertheless, our data indicated the success of carboxyl functionalization did not alter the overall morphology and mesoporous structure of MSN. Hydrodynamic diameter of the MSN-COOH was 113.41 ± 3.17 nm (Table 1), which was consistent with the size measured by TEM (~100 nm).

After being dispersed in complete medium containing 10 % FBS for 72 h, the hydrodynamic diameters of MSN-COOH particles was steady at 120 nm (Suppl. Fig. S2**A**) and the DOX release of MSN@L-K6@DOX was around 20 % (Suppl. Fig. S2**B**), suggesting a high stability and biocompatibility of MSN@L-K6@DOX.

TGA analysis was further performed to estimate the DOX and L-K6 loading in MSN@DOX and MSN@DOX@L-K6. As shown in Fig. 1**E**, the weight loss of MSN@DOX and MSN@DOX@L-K6 was approximately 24 % and 38 %, which were 13 % and 27 % higher than MSN-COOH (11 %). Additionally, the weight loss in MSN@DOX was 14 % lower than that in MSN@DOX@L-K6. All these data confirmed that DOX and L-K6 were successfully loaded on MSN-COOH.

3.2. *Drug loading/release of MSN-COOH@DOX@L-K6*

As assessed by UV–vis Spectrophotometer, under different pH conditions (7.4, 6.8 and 5.4), DOX loading for MSN@DOX@L-K6 were 23.71 %, 20.78 % and 12.86 % (w/w), respectively (standard curve as shown in Suppl. Fig. S3). A best drug loading for DOX can be found at pH = 7.4 (Table 2).

As shown in Fig. 1**F**, after 20 h incubation at pH 7.4, 6.8 and 5.4, the release of DOX from MSN@L-K6@DOX was 18.3 %, 53.6 % and 73.4 %, respectively. The drug release tended to be declined as evidenced by a less than 6 % of DOX release after 45 h (data not shown). The major reason for DOX release from MSN-COOH might be due to the weakened interactions between positively charged DOX and negatively charged MSN-COOH under different pH conditions.

Much more interestingly, we found an excellent property of pH-responsive drug release for MSN@L-K6@DOX. Under the acidic microenvironment, which favorites the growth and invasion of solid tumor (Wojtkowiak et al., 2012; Estrella et al., 2013), the DOX release was increased. This property predicted a specific toxicity of MSN@L-K6@DOX against cancer cells.

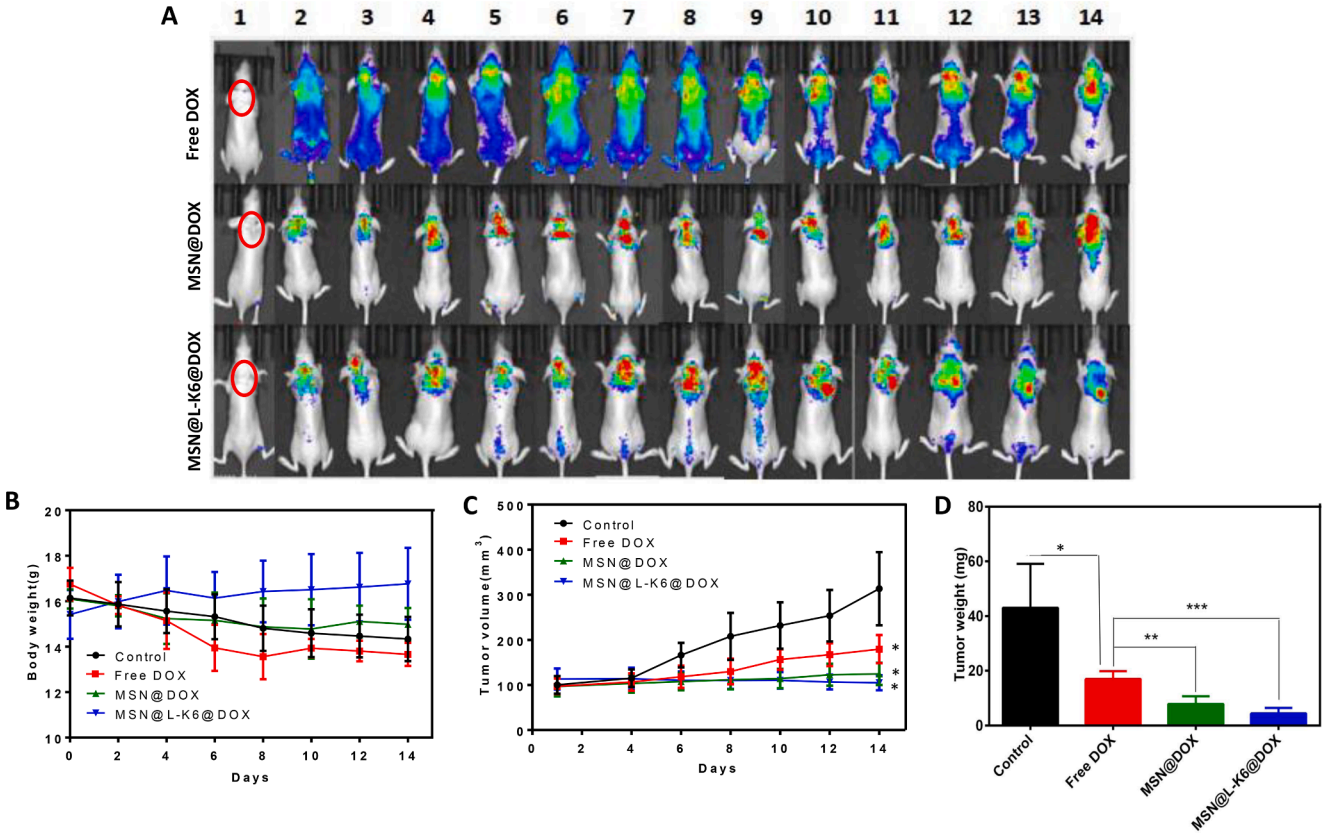

Fig. 4. DOX distribution (A) and anticancer activity assessment (B, C, D) in vivo using zenograft model mice.

3.3. *In vitro cellular uptake of DOX*

Cellular uptake of different concentrations of free DOX, MSN@DOX and MSN@L-K6@DOX in MCF-7/ADR cells after 24 h incubation was evaluated using confocal microscopy (Fig. 2**A**). As expected, MCF-7/ADR cells were resistant to DOX, as shown by the weak red fluorescence (Fig. 2**A** left panel). This resistance can be partially reversed by MSN@DOX, evidenced by the increased DOX fluorescence density (Fig. 2**A** middle panel). MSN@L-K6@DOX treatment induced a dramatic increase of intracellular uptake of DOX in a dose dependent manner (Fig. 2**A** right panel). The ameliorated intracellular accumulation of DOX after MSN@DOX and MSN@L-K6@DOX treatment could be attributed to their high positive charge, allowing more interactions between positive charged MSN@DOX and negatively charged cancer cell membrane (Motomura et al., 2018; Wang et al., 2017; Wang et al., 2016; Iwasaki et al., 2009). Additionally, the better performance of MSN@L-K6@DOX than either free DOX or MSN@DOX might be due to its P-gP inhibiting activity. As shown in Fig. 2**B**, MSN@L-K6@DOX exposure decreased the expression level of P-gP in a dose-dependent manner ($p < 0.05$ or 0.01, compared with control group). DOX as the substrate of P-gP, one multidrug efflux pump protein, can be fluxed out of cells. In MDR cancer cells, the level of P-gP protein is higher than that of both non-MDR cells, which leading to insufficient anticancer benefits. The MSN@L-K6 group dramatically depressed the P-gP protein level, thereby inhibited the P-gP-mediated efflux of DOX, increased its intracellular accumulation, and finally reversed MDR and improved the anticancer effect of DOX in MCF-7/ADR cells.

Consistent with confocal microscopy observation, quantitative analysis by flow cytometry confirmed higher intracellular DOX fluorescence density in MSN@DOX or MSN@L-K6@DOX treated cells (Fig. 2**C**). Moreover, MSN@L-K6@DOX exhibited a much better performance than MSN@DOX, with a 1.5- and 1.4-fold increase of fluorescence at 40 and 80 μg/mL, respectively (Fig. 2**D**). This elevated cellular uptake of DOX in MSN@L-K6@DOX was further confirmed by microplate assay (Suppl. Fig. S4).

3.4. *Cytotoxicity of MSN@L-K6@DOX in MCF-7 and MCF-7/ADR cells*

MCF-7/ADR cells were incubated with various concentrations of DOX, MSN-COOH, MSN@DOX or MSN@L-K6@DOX for 24, 48 and 72 h. MCF-7 cells were incubated for 4 and 24 h. Cells viability was determined using MTT assay. As shown in Fig. 3, while 24 h MSN-COOH exposure induced no obvious toxicity in MCF-7/ADR (Fig. 3**A**) and MCF-7 cell (Fig. 6**E**), significant cell death was observed after exposure of DOX, MSN@DOX and MSN@L-K6@DOX in both cell lines (Fig. 3**B-D** and Fig. 3**F-G**). Moreover, as expected, compared to MCF-7 cells, the P-gP over-expressed MCF-7/ADR cells were relatively resistant to DOX-induced toxicity, as evidenced by the increased IC_{50} values (Suppl. Table S1).

Consistent with the increased intracellular accumulation of DOX, the resistance of MCF-7/ADR cells to DOX can be reversed by exposures of MSN@DOX and MSN@L-K6@DOX, with MSN@L-K6@DOX more potent. This potentiated cytotoxicity and MDR reversal activity by MSN@DOX and MSN@L-K6@DOX was generally attributed to following factors: the enhanced permeability and retention effect of MSNs (Sun et al., 2016; Shi et al., 2020; Maeda et al., 2013), the cancer targeting and cell-penetration of L-K6 peptide (Dong et al., 2020), and the P-gP inhibiting activity (Fig. 2**B**).

3.5. *The in vivo distribution, anticancer and MDR reversal activities of MSN@DOX and MSN@L-K6@DOX in xenograft tumor model mice*

To confirm that the cancer targeting property of dual-loaded MSNs result in greater in vivo anticancer activities, we assessed DOX distribution in nude mice bearing MCF-7/ADR cells on their right flank. Xenograft model mice were intravenously administered DOX or DOX-

loaded MSNs, and the in situ particle distributions inside mice were assessed by IVIS spectrum imaging system (IVIS Lumina III, PerkinElmer, USA). As shown in Fig. 4**A**, DOX showed a dispersed distribution after repeated treatment, whereas DOX loaded MSNs exerted a cancer targeting distribution. Moreover, DOX level in MSNs treated mice, especially MSN@L-K6@DOX, was higher than that in DOX treated mice, as evidenced by the increased DOX red fluorescence.

Much more importantly, consistent with in vitro cytotoxicity, in vivo data further confirmed the anticancer and MDR reversal effects of MSN@L-K6@DOX. While no obvious body weight changes were observed (Fig. 4**B**), a significant decrease of tumor size (Fig. 4**C**) and tumor weight (Fig. 4**D**) were recorded in tumor bearing xenograft model mice. This rapid growth of tumor was inhibited by repeated treatment of DOX, and almost completely halted by DOX-loaded MSNs.

4. Conclusion

In our present study, we constructed a DOX and L-K6 dual-loaded MSNs nanocarrier. This biomaterial showed good biocompatibility, drug loading and encapsulation efficiency, as well as a pH sensitive drug release. Functionally, this dual-functionally loaded MSN delivery system with positively charged L-K6 antimicrobial peptide can preferentially target tumor cells, through electrostatic action, change the permeability of cell membrane, and reduce P-gP expression. Moreover, it was found that in acidic tumor microenvironment, the electrostatic interaction between positively charged DOX and loaded MSN-COOH is weakened. All these properties and advantages may favor the uptake and accumulation of DOX in cancer cells, thereby reversing MDR in the cancer both in vivo and in vitro. In vivo mouse experiments with subcutaneous zenograft tumors further showed that dual-loaded MSNs reach the tumor site and accumulated at higher concentrations than free DOX treatment. These findings indicate broad potential biomedical applications of this dual-loaded functionalized MSNs.

Declaration of interest

The authors declare no potential conflict of interests.

CRediT authorship contribution statement

Haiting Sun: Investigation, Methodology, Writing – original draft. **Shaodan Dong:** Data curation, Formal analysis, Investigation, Methodology, Writing – review & editing. **Lingying Kong:** Investigation. **Rongchun Wang:** Investigation. **Jiaqi Zhao:** Data curation, Investigation. **Yue Guan:** Methodology. **Che Wang:** Conceptualization, Funding acquisition, Supervision, Writing – review & editing. **Dejing Shang:** Project administration, Supervision.

Declaration of competing interest

The authors declare that they have no known competing financial interests or personal relationships that could have appeared to influence the work reported in this paper.

Acknowledgements

This work was supported by the Natural Science Foundation of Liaoning Provincial Department of Science and Technology, China (2019-ZD-0467 and 20180550306); National Natural Science Foundation of China, China (32170499, 81202448, 32070440, and 31272314); Science Research Fund of Liaoning Provincial Education Department (L2012382, L201683653); the Program for Liaoning Innovative Research Team in University (LT2012019).

Appendix A. Supplementary data

Supplementary data to this article can be found online at https://doi.org/10.1016/j.arabjc.2024.105735.

References

Cao, A., Ma, P., Yang, T., et al., 2019. Multifunctionalized micelles facilitate intracellular doxorubicin delivery for reversing multidrug resistance of breast cancer. Mol. Pharm. 16 (6), 2502–2510. https://doi.org/10.1021/acs.molpharmaceut.9b00094.

Ding, J., Yao, J., Xue, J., et al., 2015. Tumor-homing cell-penetrating peptide linked to colloidal mesoporous silica encapsulated (-)-epigallocatechin-3-gallate as drug delivery system for breast cancer therapy in vivo. ACS Appl. Mater. Interfaces 7 (32), 18145–18155. https://doi.org/10.1021/acsami.5b05618.

Dong, W., Wen, J., Li, Y., Wang, C., Sun, S., Shang, D., 2020. Targeted antimicrobial peptide delivery in vivo to tumor with near infrared photoactivated mesoporous silica nanoparticles. Int. J. Pharm. 588, 119767 https://doi.org/10.1016/j.ijpharm.2020.119767.

Duan, C.Y., Yu, M.J., Xu, J.Y., Li, B.Y., Zhao, Y., Kankala, R.K., 2023. Overcoming cancer multi-drug resistance (MDR): reasons, mechanisms, nanotherapeutic solutions, and challenges. Biomed. Pharmacother. 162, 114643 https://doi.org/10.1016/j.biopha.2023.114643.

Estrella, V., Chen, T., Lloyd, M., et al., 2013. Acidity generated by the tumor microenvironment drives local invasion. Cancer Res. 73 (5), 1524–1535. https://doi.org/10.1158/0008-5472.CAN-12-2796.

Halder, J., Pradhan, D., Kar, B., Ghosh, G., Rath, G., 2022. Nanotherapeutics approaches to overcome P-glycoprotein-mediated multi-drug resistance in cancer. Nanomedicine 40, 102494. https://doi.org/10.1016/j.nano.2021.102494.

Hu, Y., Ke, L., Chen, H., et al., 2017. Improved gene transfer with functionalized hollow mesoporous silica nanoparticles of reduced cytotoxicity. Int. J. Nanomed. 12, 8411–8426. https://doi.org/10.3390/ma10070731.

Huang, I.P., Sun, S.P., Cheng, S.H., et al., 2011. Enhanced chemotherapy of cancer using pH-sensitive mesoporous silica nanoparticles to antagonize P-glycoprotein-mediated drug resistance. Mol. Cancer Ther. 10 (5), 761–769. https://doi.org/10.1158/1535-7163.

Huo, Q.S., 2011. Synthetic chemistry of the inorganic ordered porous materials. Mod. Inorg. Synth. Chem. 339–373. https://doi.org/10.1016/B978-0-444-63591-4.00015-X.

Iwasaki, T., Ishibashi, J., Tanaka, H., et al., 2009. Selective cancer cell cytotoxicity of enantiomeric 9-mer peptides derived from beetle defensins depends on negatively charged phosphatidylserine on the cell surface. Peptides 30 (4), 660–668. https://doi.org/10.1016/j.peptides.2008.12.019.

Jemal, A., Siegel, R., Ward, E., Hao, Y., Xu, J., Thun, M.J., 2009. Cancer statistics, 2009. CA Cancer J. Clin. 59 (4), 225–249. https://doi.org/10.3322/caac.20006.

Li, X., Wu, X., Yang, H., Li, L., Ye, Z., Rao, Y., 2019. A nuclear targeted Dox-aptamer loaded liposome delivery platform for the circumvention of drug resistance in breast cancer. Biomed. Pharmacother. 117, 109072 https://doi.org/10.1016/j.biopha.2019.109072.

Maeda, H., Nakamura, H., Fang, J., 2013. The EPR effect for macromolecular drug delivery to solid tumors: improvement of tumor uptake, lowering of systemic toxicity, and distinct tumor imaging in vivo. Adv. Drug Deliv. Rev. 65 (1), 71–79. https://doi.org/10.7150/thno.49577.

Motomura, M., Ichihara, H., Matsumoto, Y., 2018. Nano-chemotherapy using cationic liposome that strategically targets the cell membrane potential of pancreatic cancer cells with negative charge. Bioorg. Med. Chem. Lett. 28 (7), 1161–1165. https://doi.org/10.1016/j.bmcl.2018.03.013.

Murugan1 C, Rayappan1 K, Thangam R, et al. Combinatorial nanocarrier based drug delivery approach for amalgamation of anti-tumor agents in bresat cancer cells: an improved nanomedicine strategies. Sci. Rep., 2016; 6. 34053. Doi: 10.1038/srep34053.

Pan, Y., Zhou, S., Li, Y., Parshad, B., Li, W., Haag, R., 2021. Novel dendritic polyglycerol-conjugated, mesoporous silica-based targeting nanocarriers for co-delivery of doxorubicin and tariquidar to overcome multidrug resistance in breast cancer stem cells. J. Control. Release 330, 1106–1117. https://doi.org/10.1016/j.jconrel.2020.11.015.

Shen, J., He, Q., Gao, Y., Shi, J., Li, Y., 2011. Mesoporous silica nanoparticles loading doxorubicin reverse multidrug resistance: performance and mechanism. Nanoscale 3 (10), 4314–4322. https://doi.org/10.1039/c1nr10580a.

Shi, Y., van der Meel, R., Chen, X., Lammers, T., 2020. The EPR effect and beyond: strategies to improve tumor targeting and cancer nanomedicine treatment efficacy. Theranostics. 10 (17), 7921–7924. https://doi.org/10.7150/thno.49577.

Siegel, R.L., Miller, K.D., Fuchs, H.E., Jemal, A., 2021. Cancer statistics, 2021. CA Cancer J. Clin. 71 (1), 7–33. https://doi.org/10.3322/caac.21654.

Sun, W., Han, Y., Li, Z., Ge, K., Zhang, J., 2016. Bone-targeted mesoporous silica nanocarrier anchored by zoledronate for cancer bone metastasis. Langmuir 32 (36), 9237–9244. https://doi.org/10.1021/acs.langmuir.6b02228.

Szakács, G., Paterson, J.K., Ludwig, J.A., Booth-Genthe, C., Gottesman, M.M., 2006. Targeting multidrug resistance in cancer. Nat. Rev. Drug Discov. 5 (3), 219–234. https://doi.org/10.1038/nrd1984.

Varshosaz, J., Taymouri, S., 2015. Hollow inorganic nanoparticles as efficient carriers for siRNA delivery: a comprehensive review. Curr. Pharm. Des. 21 (29), 4310–4328. https://doi.org/10.2174/1381612821666150901103937.

Wang, C., Chen, Y.W., Zhang, L., Gong, X.G., Zhou, Y., Shang, D.J., 2016. Melanoma cell surface-expressed phosphatidylserine as a therapeutic target for cationic anticancer

peptide, temporin-1CEa. J. Drug Target 24 (6), 548–556. https://doi.org/10.3109/1061186X.2015.1113539.

Wang, C., Dong, S., Zhang, L., et al., 2017. Cell surface binding, uptaking and anticancer activity of L-K6, a lysine/leucine-rich peptide, on human breast cancer MCF-7 cells. Sci. Rep. 7 (1), 8293. https://doi.org/10.1038/s41598-017-08963-2.

Wang, C., Huang, L.L., Li, R.J., Wang, Y., Wu, X.X., Shang, D.J., 2021. Synergistic therapy of doxorubicin with cationic anticancer peptide L-K6 reverses multidrug resistance in MCF-7/ADR cancer cells in vitro via P-glycoprotein inhibition. Int. J. Pept. Res. Ther. 27, 2291–2301. https://doi.org/10.1007/s10989-021-10253-5.

Wang, H., Zhao, Y., Wang, H., et al., 2014. Low-molecular-weight protamine-modified PLGA nanoparticles for overcoming drug-resistant breast cancer. J. Control. Release 192, 47–56. https://doi.org/10.1016/j.jconrel.2014.06.051.

Wojtkowiak, J.W., Rothberg, J.M., Kumar, V., et al., 2012. Chronic autophagy is a cellular adaptation to tumor acidic pH microenvironments. Cancer Res. 72 (16), 3938–3947. https://doi.org/10.1158/0008-5472.CAN-11-3881.

Xu, Z.P., Zeng, Q.H., Lu, G.Q., Yu, A.B., 2006. Inorganic nanoparticles as carriers for efficient cellular delivery. Chem. Eng. Sci. 61 (3), 1027–1040. https://doi.org/10.1016/j.ces.2005.06.019.

Zeng, X.W., Liu, G., Tao, W., et al., 2017. Cancer therapy: a drug-self-gated mesoporous antitumor nanoplatform based on pH-sensitive dynamic covalent bond. Adv. Funct. Mater. 27 (11), 1605985. https://doi.org/10.1002/adfm.201770065.

Zhao, X., Chen, Q., Li, Y., Tang, H., Liu, W., Yang, X., 2015. Doxorubicin and curcumin co-delivery by lipid nanoparticles for enhanced treatment of diethylnitrosamine-induced hepatocellular carcinoma in mice. Eur. J. Pharm. Biopharm. 93, 27–36. https://doi.org/10.1016/j.ejpb.2015.03.003.